International Journal of Greenhouse Gas Control 44 (2016) 166–174

Contents lists available at ScienceDirect

International Journal of Greenhouse Gas Control

journal homepage: www.elsevier.com/locate/ijggc

Mineral dissolution and precipitation during CO_2 injection at the Frio-I Brine Pilot: Geochemical modeling and uncertainty analysis

A.G. Ilgen*, R.T. Cygan

Sandia National Laboratories, Geochemistry Department, Albuquerque, NM, 87185-0754, United States

ARTICLE INFO

Article history:
Received 25 August 2015
Received in revised form
13 November 2015
Accepted 17 November 2015

Keywords:
CO_2 geologic storage
Saline aquifers
Mineral trapping
Dissolution
Pyrite
Calcite

ABSTRACT

During the Frio-I Brine Pilot CO_2 injection experiment in 2004, distinct geochemical changes in response to the injection of 1600 tons of CO_2 were recorded in brine samples collected from the monitoring well. Previous geochemical modeling studies have considered dissolution of calcite and iron oxyhydroxides, or release of adsorbed iron, as the most likely sources of the increased ion concentrations. In this modeling study we explore possible alternative sources of the increasing calcium and iron, based on the data from the detailed petrographic characterization of the Upper Frio Formation "C". Particularly, we evaluate whether dissolution of pyrite and oligoclase (anorthite component) can account for the observed geochemical changes. Due to kinetic limitations, dissolution of pyrite and anorthite cannot account for the increased iron and calcium concentrations on the time scale of the field test (10 days). However, dissolution of these minerals is contributing to carbonate and clay mineral precipitation on the longer time scales (1000 years). We estimated that during the field test dissolution of calcite and iron oxide resulted in ~0.02 wt.% loss of the reservoir rock mass. The reactive transport models were constructed for 25 and 59 °C temperature and using Pitzer and B-dot activity correction methods. These models predict carbonate minerals, dolomite and ankerite, as well as clay minerals kaolinite, nontronite and montmorillonite, will precipitate in the Frio Formation "C" sandstone as the system progresses toward chemical equilibrium during a 1000-year period. Cumulative uncertainties associated with using different thermodynamic databases, activity correction models (Pitzer vs. B-dot), and extrapolating to reservoir temperature, are manifested in the difference in the predicted mineral phases. However, these models are consistent with regards to the total volume of mineral precipitation and porosity values which are predicted to within 0.002%.

1. Introduction

Geological carbon storage (GCS) in the subsurface, particularly in deep permeable saline formations, is one of the feasible methods for decreasing atmospheric carbon dioxide (CO_2) and mitigating its impact on global climate (DePaolo et al., 2013; Kharaka and Cole, 2011; Kobos et al., 2011; Marini, 2006; Steele-MacInnis et al., 2012). Natural analogs for CO_2 storage are stable and are capable of retaining CO_2 on geologic time scales (Marini, 2006; Sathaye et al., 2014), with solubility trapping being the predominant sink of CO_2 (Gilfillan et al., 2009). The roles of various trapping mechanisms over time in assuring long term storage in such reservoirs are still being investigated (Bickle et al., 2013; Marini, 2006). Crucial features of these reservoirs are sufficient porosity to accommodate the required volumes of CO_2, and continuous cap rock impermeable to CO_2. Deep saline reservoirs are therefore among the top candidate formations considered for the geological storage of CO_2 (DePaolo et al., 2013; Marini, 2006).

At the deep geologic storage temperature and pressure, CO_2 is stable in its supercritical (sc) state. Emplacement of $scCO_2$ into a reservoir stimulates a geochemical response mostly driven by acidification of parent brine by CO_2 dissolution, and dehydration of mineral surfaces by the dispersing $scCO_2$ phase (DePaolo et al., 2013; Jun et al., 2012; Kharaka and Cole, 2011; Marini, 2006). Existing experimental and field studies indicate that geochemical reactions triggered by the injection of CO_2 differ significantly for different rock assemblages and brine compositions (Bickle et al., 2013; Jun et al., 2012; Lu et al., 2012). Typical low permeability cap rocks, such as shale, have been shown to be reactive at the higher end of the GCS temperature range (Kaszuba et al., 2003; Liu et al., 2012). Dissolution and re-precipitation of carbonate minerals, dissolution of feldspars, and precipitation of clay minerals are observed (Liu et al., 2012). Therefore, for some potential CO_2

* Corresponding author at: Sandia National Laboratories, Geochemistry Department, P.O. Box 5800 MS-0754, Albuquerque, NM 87185-0754, United States.
E-mail address: agilgen@sandia.gov (A.G. Ilgen).

http://dx.doi.org/10.1016/j.ijggc.2015.11.022
1750-5836/

storage reservoirs, dissolution and secondary mineral precipitation triggered by the emplacement of $scCO_2$ would ultimately control the evolution of porosity and permeability (Jun et al., 2012), with potential impact on the cap rock integrity and CO_2 leakage (Fitts and Peters, 2013; Harvey et al., 2012; Liu et al., 2012).

Thermodynamic and kinetic modeling of CO_2 sequestration is widely used to predict the geochemical response of the aquifer rocks, brines, and sealing cap rock and predict the efficiency of GCS (Fischer et al., 2012; Jun et al., 2012; Liu et al., 2011; Marini, 2006; Song and Zhang, 2012; Xu et al., 2004, 2005, 2011). Geochemical models calculate the potential for CO_2 solubility and mineral trapping in the subsurface, and are used for constructing probable scenarios for the long-term (>100 years) stability of CO_2 storage. Accuracy of these geochemical models can be limited by uncertain analytical data, incomplete thermodynamic datasets (particularly for minerals which form solid solutions), inadequate activity correction for high ionic strength brines, limited knowledge of nucleation/crystal growth and dissolution kinetics, and uncertain accessible reactive surface areas of the minerals present in aquifers and cap rocks (Haase et al., 2013; Marini, 2006; Nitzsche et al., 2000).

Large CO_2 injections into subsurface have been performed during enhanced oil or gas recovery, and smaller-scale pilot demonstration projects have also been completed (DePaolo et al., 2013). One of the short-term tests aimed at the investigation of potential CO_2 storage in the deep sedimentary formations—Frio-I Brine Pilot experiment—was conducted in 2004 (Kharaka et al., 2006). The details about Frio-I Brine Pilot experiment can be found elsewhere (Kharaka et al., 2006, 2009, 2013; McGuire, 2009). Briefly, 1600 tons of CO_2 were injected into the Frio Formation "C" sandstone at 1541–1546 m depth, for the duration of 10 days, at a rate of 3 kg s^{-1} (Kharaka et al., 2006). The monitoring well, completed about 30 m updip of the injection point, was configured at 1528–1534 m depth for brine sampling and tracking the arrival of CO_2 (Kharaka et al., 2006, 2009, 2013; McGuire, 2009). The breakthrough of CO_2 was recorded 51 h after the injection had started (Kharaka et al., 2009), and increasing alkalinity, calcium, iron, and manganese accompanied by a drop in pH were observed (Kharaka et al., 2009). These geochemical observations were attributed to the rapid dissolution of calcite (Kharaka et al., 2009), and either dissolution of iron oxyhydroxides (Kharaka et al., 2009), or release of adsorbed iron due to decreasing pH (Xu et al., 2010). Xu et al. (2010) developed comprehensive geochemical models using changes in Frio brine geochemistry in response to the $scCO_2$ injection. These models assumed the release of iron adsorbed onto the mineral grain coatings, and were calibrated to mimic the observed iron and bicarbonate increases. The long-term reactive transport model constructed to predict the behavior of CO_2 injected during Frio-I Brine Pilot predicts CO_2 transport, dissolving into the brine, and disappearing after 500 years, with all injected CO_2 sequestered as carbonate minerals (Xu et al., 2010). While calcite cement is abundant and constitutes on average 5.3 vol.% (Land, 1984) in the Frio Formation units regionally, it varies depending on the depositional environment and the degree of diagenetic cementation, and can sometimes be absent (Land, 1984). A detailed petrographic and geochemical study of the Upper Frio Formation "C", where CO_2 was injected during the Frio-I Brine pilot, found no calcite cement in this stratigraphic unit (McGuire, 2009). The Frio Formation "C" sandstone on average contains 24 wt.% of feldspar, significant portion of which is anorthite $CaAl_2Si_2O_8$, detectable by the X-ray diffraction (XRD) (McGuire, 2009). Thin clay or oxide coatings were observed on sand grains, and gradually oxidized to tan colors when core was exposed to air. No crystalline iron oxyhydroxides were detected; however abundant fine-crystalline pyrite FeS_2 was found within the pore spaces (McGuire, 2009). Pyrite is a common mineral constituent in the reservoirs and cap rocks considered for CO_2 sequestration (Kaszuba et al., 2013). There is limited data on the dissolution/precipitation of pyrite expected in response to the injection of CO_2. One experimental study of the cap rock reactivity with CO_2 indicated some pyrite dissolution and secondary siderite precipitation adjacent to the pyrite grains (Liu et al., 2012). Recent experimental work on Gothic Shale shows that pyrite dissolution is triggered by the presence of oxygen (O_2) in the reacting CO_2 mixture (Jung et al., 2013).

The focus of the present study is to explore possible alternative sources of the increasing calcium and iron in the monitoring well samples, based on the data from the detailed characterization of the Upper Frio Formation "C". In particular, the goals of our work are to (1) use thermodynamic and kinetic modeling to test the hypothesis that the increase in iron could be due to the dissolution of abundant fine-grained pyrite; and increase in calcium to dissolution of anorthite; (2) explore the range of uncertainty due to indeterminate rate constants for the pyrite, calcite, and anorthite dissolution, and compare the range of predicted values calculated using thermodynamic and kinetic modeling to the actual observations recorded during the Frio-I Brine Pilot; and (3) construct a long-term (1000 years) reactive transport model to account for precipitation of carbonates, using the detailed petrographic results on the mineral composition of the Frio Formation "C", and quantify the cumulative uncertainty of using different thermodynamic databases, activity correction models (Pitzer vs. B-dot), and extrapolation to the reservoir temperature of 59 °C.

2. Geochemical modeling methods

2.1. Frio-I Brine Pilot data

Selected geochemical data collected from the monitoring well has been discussed in a number of earlier publications (Kharaka et al., 2006, 2009, 2013; McGuire, 2009). In this work, we selected a subset of chemical data shown in Table 1, which was collected from the monitoring well prior to, during, and after the injection of CO_2. This dataset was provided by Susan Hovorka from Gulf Coast Carbon Center, Bureau of Economic Geology, Jackson School of Geosciences, University of Texas at Austin. The original sampling and chemical analysis were done by Yousif Kharaka and staff at USGS Menlo Park, CA.

2.2. Geochemical modeling

The Geochemist Workbench (GWB) software (Bethke, 2008) was used for reaction path (React module), and one-dimensional (1D) reactive transport (X1t module) modeling. The stoichiometric ionic strength of Frio native brine is 1.6 molal (Xu et al., 2010), which is outside of the optimal range for the extended Debye–Hückel (B-dot version) activity correction model for ions, other than Na^+ and Cl^- (Bethke, 2008). Therefore we also used Pitzer activity model (Pitzer, 1979) to predict activity of the aqueous species involved in carbonate and aluminosilicate mineral solubility. The Pitzer parameters were taken from a modified version of the EQ3/6 (Wolery et al., 1990) database—data0.ymp.R1, updated by Jové Colón (2005), which was converted into the GWB format. We further modified this database to exclude elements not relevant to this study (e.g. actinides). The final version includes 20 elements: aluminum (Al), boron (B), bromine (Br), carbon (C), calcium (Ca), cadmium (Cd), chlorine (Cl), fluorine (F), iron (Fe), hydrogen (H), potassium (K), lithium (Li), magnesium (Mg), manganese (Mn), nitrogen (N), sodium (Na), oxygen (O), phosphorus (P), sulfur (S), and silicon (Si). The solubility constants for the key carbonate minerals were updated based on the Gibbs free energy (G) and enthalpy (H) of formation for dolomite $CaMg(CO_3)_2$ (Holland and

Table 1
Chemical composition of the brine samples collected prior, during, and after the injection of CO_2 during the Frio-I Brine Pilot experiment. All values are given in mg L^{-1}.

Date	Site	pH	Na^+	K^+	Mg^{2+}	Ca^{2+}	Sr^{2+}	Ba^{2+}	Mn^{2+}	Fe^{2+}	Cl^-	Br^-	SO_4^{2-}	HCO_3^-	$SiO_{2(aq)}$
Before CO_2 injection															
8/1/04	Monitoring well	7.2	31,827	175	501	2934	121	91	2.5	29	54,974	74	12	130	26
8/1/04	Monitoring well	7.2	32,554	178	524	3022	126	98	2.6	30	56,335	71	3.8	131	28
8/2/04	Monitoring well	6.7	32,143	185	524	3075	128	101	2.6	24	56,089	69	5.0	135	31
	Average	7.0	31,175	179	516	3010	125	97	2.6	28	55,799	71	7.0	132	28
During CO_2 injection															
10/05/04	Monitoring well[a]	6.5	30,550	175	516	2822	118	91	3.1	41	53,254	68		37	n/a
10/06/04	Monitoring well[a]	6.4	30,627	168	524	2823	118	92	3.1	34	52,934	68	4.2	60	n/a
10/06/04	Monitoring well[a]	6.6	30,597	180	522	2889	118	92	3.0	13	52,701	69	4.6	31	n/a
10/06/04	Monitoring well[a]	6.3	30,909	173	523	2807	118	91	3.2	22	52,370	68	4.6	44	n/a
10/06/04	Monitoring well[a]	5.8	31,505	170	540	3243	128	93	5.1	207	52,648	67	5.0	1230	n/a
10/06/04	Monitoring well[a]	5.8	30,979	173	528	3271	128	93	7.0	314	52,265	67	5.5	2100	n/a
10/06/04	Monitoring well[a]	5.7	30,775	169	524	3183	125	93	9.5	482	51,948	67	5.3	2140	66
10/06/04	Monitoring well[a]	5.8	30,366	171	525	3067	123	92	12	614	52,539	68		2180	71
10/07/04	Monitoring well[a]	5.9	30,583	171	539	3101	125	91	17	925	53,212	70	4.7	2710	63
10/07/04	Monitoring well[a]	5.9	30,305	172	535	3076	122	86	18	847	53,139	67		2760	61
10/07/04	Monitoring well[a]	6.0	31,177	174	537	3062	122	94	18	1115	53,041	68	4.3	2980	70
After CO_2 injection															
10/29/04	Monitoring well[a]	5.8	30,897	179	529	2833	119	95	6.1	391	52,920	68	4.9	1169	66
10/29/04	Monitoring well[a]	5.7	30,868	181	543	2917	122	96	6.1	370	53,685	69	5.2	1120	64
11/03/04	Monitoring well[a]	5.7	30,276	181	523	2863	118	95	6.2	540	52,833	68	4.9	1477	73
11/03/04	Monitoring well[a]	5.7	31,058	180	536	2891	119	96	6.0	437	53,205	68	4.7	1273	66

[a] U-tube sampler.

Powell, 1998), magnesite $MgCO_3$ (Holland and Powell, 1998), hydromagnesite $Mg_5(CO_3)_4(OH)_2{\cdot}4H_2O$ (Robie and Hemingway, 1995), dawsonite $NaAlCO_3(OH)_2$ (Bénézeth et al., 2007), siderite $FeCO_3$ (Bénézeth et al., 2009), and ΔG and ΔH values for bicarbonate HCO_3^- species were updated (Robie and Hemingway, 1995). We also added ankerite $CaFe(CO_3)_2$ (Holland and Powell, 1998) to the database. The solubility constants for pyrite FeS_2 and anorthite $CaAl_2Si_2O_8$ were added from the *thermo.dat* database included in the GWB package. Pitzer parameters are represented by the four-term temperature function given by:

$$x(T) = a1 + a2\left(\frac{1}{T} - \frac{1}{298.15}\right) + a3\ln\left(\frac{T}{298.15}\right) + a4(T - 298.15) \quad (1)$$

where T is temperature in Kelvin and $a1$ through $a4$ denote the fitting coefficients for the temperature dependent Pitzer parameters. Ionic composition of Frio brine is dominated by Na^+ (1.35 molal) and Cl^- (1.49 molal) (Xu et al., 2010), therefore ion-specific interactions are dominated by the interactions with Cl^- and Na^+ accounted by the Pitzer activity model. Coefficients $a1$ through $a4$ for temperature extrapolation in Eq. (1) are available for some relevant ion pairs, for example, Ca^{2+}/Cl^-, $CaCl^+/Cl^-$, Na^+/Cl^-, Mg^{2+}/Cl^-, Na^+/CO_3^{2-}, Na^+/HCO_3^-, Fe^{2+}/Cl^-, while not available for others, for example for Al^{3+}/Cl^-, and Mn^{2+}/Cl^-, therefore extrapolation to temperatures above 25 °C is valid only for a select number of mineral components, which includes calcite. Taking this limitation into account, we ran some simulations at two temperatures: 25 °C (no extrapolation of thermodynamic data) and 59 °C (extrapolation to the reported reservoir temperature), while other simulations were studied only at 25 °C. This work focuses on mineral dissolution and precipitation, therefore adsorption processes are not accounted for in our models.

2.2.1. Reaction path models

Reaction path modeling was used to predict solution composition, shifts in pH, and mineral saturation as a function of reaction progress, that is, the environmental response to $scCO_2$ emplacement in the reservoir. The simulations involved reactants being titrated into the system with initial aqueous composition of the brine (Table 1, average values calculated for the "Before CO_2 injection" section), and chemical and redox (Fe^{2+}/Fe^{3+}, HS^-/SO_4^{2-}couples) equilibria were assumed to be reached at each step, unless specified otherwise. Relevant minerals were allowed to precipitate instantaneously, while kinetic rate parameters were specified for dissolution, unless stated otherwise for a given model. The maximum concentration of dissolved CO_2 was calculated using CO_2 solubility model developed by Duan and Sun (2003). For the Frio brine composition (assuming NaCl concentration of 1.6 mol kg^{-1} H_2O—the reported stoichiometric ionic strength for Frio brine), pressure (152 bars), and temperature (333.15 K) the maximum dissolved CO_2 is calculated at 0.82 mol kg^{-1}.

The maximum concentration of O_2 dissolved in the Frio brine was calculated based on the solubility data from Geng and Duan (2010). Food-grade CO_2 was used during the Frio-I Pilot (Kharaka et al., 2013), and this CO_2 grade is reported to have 50 ppm of O_2 (from Matheson "Food and Beverage Grade Gas Manual"). At the 50 ppm O_2 concentration in the CO_2 mixture and for the Frio brine composition, temperature, and pressure listed above, the calculated concentration of dissolved oxygen is 3.5×10^{-6} mol kg^{-1}.

2.2.2. Reactive transport model

The radial 1D reactive transport models were constructed to predict the long-term mineral dissolution and precipitation after the emplacement of CO_2 in the geochemical conditions representative of the Frio Formation "C" reservoir. We did not account for the local reservoir geometry or potential preferential flow behavior. The flow rate for the Frio "C" unit was estimated at 0.3–0.4 m/day, given the reported geometry (Doughty et al., 2008) (8 m unit thickness, and 30 m distance between the injection and monitoring well), CO_2 arrival time, and reported porosity of 24% (McGuire, 2009) to 36% (Doughty et al., 2008). The "inlet" concentrations of the geochemical basis species are listed in Table 1 (average values calculated for the "Before CO_2 injection" section, Al^{3+} concentration was set at 1.56×10^{-8} mol kg^{-1}, consistent with Xu et al. (2010). The representative models were constructed as a solid block of 30-m length initially containing Frio brine saturated with CO_2 ("Composition of the Frio-I brine reacted with CO_2", Table 2). The block was flushed with the "Before CO_2 injection" fluid composition (Table 1), for 1000 years duration of the simulation. Horizontal position of 29.5 m from the inlet was selected for the discussion of the final modeling results. Four reactive transport models were constructed using two temperatures and two thermodynamic databases. These

Table 2
Input for the 1D reactive flow model: (a) calculated chemical composition of the Frio-I brine samples after the equilibration with the injected CO_2; (b) minerals allowed to react, mineral surface areas, and kinetic dissolution rate constants.

(a) Composition of the Frio-I brine reacted with CO_2, mg L^{-1}

pH	Na^+	K^+	Mg^{2+}	Ca^{2+}	Fe^{2+}	Cl^-	SO_4^{2-}	HCO_3^-	$SiO_{2(aq)}$	$CO_{2(aq)}$
3.3	31,670	181	532	2920	31.8	55,768	6.7	73.7	17.6	36,048

(b) Minerals considered in the 1D reactive flow model

Mineral	Vol.% of solid	A, $cm^2\ g^{-1}$	k, mol $cm^{-2}\ s^{-1}$	Mineral	Vol.% of solid	A, $cm^2\ g^{-1}$	k, mol $cm^{-2}\ s^{-1}$
Quartz	44	10	1.023×10^{-18}	Calcite	0.0056	10	5.012×10^{-10}
K-Feldspar	12	10	3.89×10^{-17}	Albite	6.2	10	1.445×10^{-16}
Anorthite	1.6	10	2.1×10^{-16}	Pyrite	1.0	500	2.79×10^{-15}

models are: (1) temperature 25 °C, Pitzer thermodynamic database, (2) temperature 59 °C, Pitzer thermodynamic database; (3) temperature 25 °C, B-dot (thermo.dat) thermodynamic database, and (4) temperature 59 °C, B-dot (thermo.dat) thermodynamic database. These conceptual models captured the period of system "relaxation" following the injection of CO_2 when brine is allowed to flush the reservoir saturated with CO_2. Similar to the reaction path models, chemical and redox (Fe^{2+}/Fe^{3+} couple) equilibria were assumed to be reached at each step. Kinetic rate laws were specified for the dissolution of the relevant minerals (Table 2), unless stated otherwise.

2.2.3. Uncertainty analysis and mineral dissolution

Uncertainty in modeling calcite dissolution was quantified taking into account uncertainties associated with the calcite dissolution rate constant (Arvidson et al., 2003) and the mass of calcite available for reaction. The specific surface area of calcite was kept constant at 10 $cm^2\ g^{-1}$. The relevant calcite dissolution rate constants were taken from the compilation of experimentally determined calcite dissolution rates by Arvidson et al. (2003), and varied between $k = 10^{-10}$ mol $cm^{-2}\ s^{-1}$ and $k = 10^{-8}$ mol $cm^{-2}\ s^{-1}$ for the relevant pH range. The average primary porosity of the Frio Formation "C" sandstones is 24% (±11) (McGuire, 2009). Our geochemical model considers 1 kg of solvent and, when porosity is taken into account, the solid mass needed to accommodate 1 kg of solvent is ~8.9 kg (considering the mean solid phase density equal to the density of quartz, 2.65 g cm^{-3}). Assuming the trace amounts of calcite are on the order of 0.001–0.1 wt.%, the resulting calculated mass of calcite varies from 0.09 to 9.0 g, respectively. We also assume that the trace amounts of calcite are concentrated at the mineral grain boundaries and are available to react with the brine saturated with CO_2. Therefore, in our uncertainty estimation we varied the total amount of available calcite from 0.09 to 9.0 g. We also compared how the results of the reaction path model change as a function of temperature, and performed our calculations at both 25 and 59 °C.

A similar approach was used to quantify the uncertainty associated with modeling the dissolution of plagioclase. Plagioclase in Frio sandstones has an average oligoclase composition with the representative anorthite ($CaAl_2Si_2O_8$) to albite ($NaAlSi_3O_8$) ratio of 1:4 (Xu et al., 2010). The maximum and minimum values for the dissolution rate of the relevant oligoclase solid solution (An_{20}) were taken from Stillings and Brantley (1995). The rate constant for An_{20} at pH 3 varies from $10^{-14.8}$ to $10^{-15.5}$ mol $cm^{-2}\ s^{-1}$ (Stillings and Brantley, 1995). Given the above calculated mass of solid of 8.9 kg, and reported mean composition of the Frio Formation "C" sandstone $Q_{70}F_{24}L_6$ (Q = quartz; F = feldspars, L = lithics) (McGuire, 2009), and assuming K-feldspar at 15.9 wt.% of the total solids, we calculated that roughly 153 g of anorthite, and 612 g of albite, should be present in a sandstone comprised of 8.9 kg of solids. The specific surface area of anorthite and albite was kept constant at 10 $cm^2\ g^{-1}$. The uncertainty range for the plagioclase dissolution models was therefore estimated by using the higher ($k = 10^{-14.8}$ mol $cm^{-2}\ s^{-1}$) and lower ($k = 10^{-15.5}$ mol $cm^{-2}\ s^{-1}$) values for the kinetic rate constant.

Pyrite dissolution is a redox sensitive reaction, which contributes to the uncertainty in constraining its kinetic parameters. There are several chemical pathways of the oxidative dissolution of pyrite (Druschel and Borda, 2006). Briefly, dissolved oxygen (O_2), ferric iron (Fe^{3+}), and potentially other aqueous species can oxidize pyrite and promote its dissolution. In the reaction path models we use a kinetic rate law with the kinetic rate constant calculated based on Williamson and Rimstidt (1994):

$$r = 10^{-8.19(\pm 0.10)} \frac{m_{DO}^{0.5(\pm 0.04)}}{m_{H+}^{0.11(\pm 0.01)}} \quad (\text{mol m}^{-2}\ \text{s}^{-1}) \tag{2}$$

Based on the predicted dissolved oxygen content of 3.5×10^{-6} m, and pH of 3.3, the calculated rate constant is 2.65×10^{-11} mol $m^{-2}\ s^{-1}$. This rate constant is used in both reaction path and reactive transport models.

To evaluate the range of uncertainty associated with modeling the dissolution of pyrite, we took into account uncertainties in (1) Eq. (2); (2) the kinetic rate constants reported in literature, in particular, tested a case where the rate constant was set at the value from Xu et al. (2010); and (3) available mass of pyrite. The available mass of pyrite was initially set at 9.8 g, which is calculated using the reported average of pyrite comprising 1% of the total volume in Frio C sandstone (McGuire, 2009). The reported variability of pyrite in Frio C sandstone is 0–12 vol.% (McGuire, 2009), therefore, we also tested a model where 117 g of pyrite was available corresponding to the maximum value of 12 vol.%. We estimated the total surface area of pyrite at 998 $cm^2\ g^{-1}$ using the reported pyrite geometry (10–15 μm spheres) (McGuire, 2009). Since this framboidal pyrite is reported to line and bridge pores (McGuire, 2009), it is expected to be accessible to the fluids. Therefore we assumed that about 50% of the total surface area is accessible, and set the reactive surface area of pyrite at 500 $cm^2\ g^{-1}$. Similar to Xu et al. (2010), we assumed that the increase in Fe^{2+} is predominantly due to its release from the sediment, as a result of the reaction with the CO_2-charged brine, and any contribution from the metal well casing is insignificant.

The cumulative uncertainty in the reactive transport model was quantified by comparing the total mass of minerals predicted to precipitate in four models, calculated using two different thermodynamic databases at two temperatures (25 and 59 °C). One thermodynamic database is thermo.dat (Bethke, 1998), which uses B-dot activity correction model; the other is the Pitzer-model database described in Section 2.

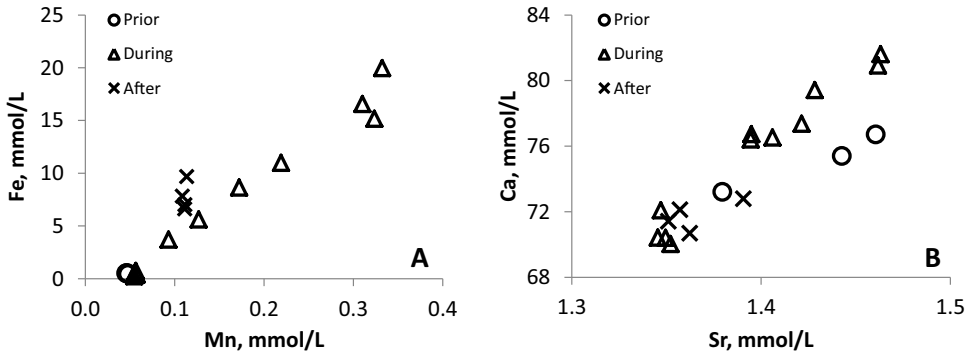

Fig. 1. Positive correlation between iron/manganese, and calcium/strontium observed in the samples collected from the monitoring well prior, during, and after the injection of CO_2. (A) Linear correlation between Fe and Mn may indicate the same source—Mn-enriched pyrite found in the Frio "C" sandstones (McGuire, 2009); (B) Ca and Sr are strongly correlated, likely due to the dissolution of Ca-containing mineral phase.

3. Results and discussion

3.1. Source of calcium and iron in brine samples

We observed linear correlations between increasing Fe and Mn, as well as between Ca and Sr concentrations, in the monitoring well samples collected during the injection of CO_2 (Fig. 1). These correlations may indicate the mineral sources from which these elements are released. Detailed petrographic and geochemical analysis of the upper Frio Formation "C" sandstone suggest that both euhedral and framboidal pyrite occur ubiquitously, with Mn content up to 4 wt.%, with an average of 1 wt.% (McGuire, 2009). Macroscopic observations of pyrite dissolution in acidic media imply an incongruent process with the resulting concentration of released sulfate being lower than what would be expected given the stoichiometry of pyrite (Descostes et al., 2004; Druschel and Borda, 2006). Therefore, the absence of linear correlation between iron and sulfate concentrations recorded in the monitoring well samples during the CO_2 injection can be explained by the incongruent nature of pyrite dissolution. Depending on the reaction pathway, this low sulfur recovery can be due to its partial conversion into elemental form S^0, which takes place after sulfur detachment from the surface of dissolving pyrite (Descostes et al., 2004; Druschel and Borda, 2006).

Strontium commonly substitutes for calcium in the structure of calcite and can substitute for calcium in anorthite during plagioclase crystallization (Drake and Weill, 1975). No calcite was detected by the petrographic examination of the Upper Frio Formation "C" sandstones (McGuire, 2009), while anorthite was detectable by XRD (McGuire, 2009). Unlike Fe and Mn, the concentrations of Ca and Sr in the monitoring well samples were not increasing continuously during the injection of CO_2; they increased during the first half of the Frio experiment and then dropped off (Fig. 2). Also, Ca and Sr concentrations had an inverse linear correlation with the measured pH for the first half of the CO_2 injection experiment, and did not correlate with the pH when Ca and Sr concentrations were decreasing. One explanation for these concentration changes is that minor amounts of calcite were encountered by the brine/CO_2 plume and were completely dissolved (hence, initial increase followed by the decrease in Ca and Sr concentrations) even though calcite was undetected in the samples examined by McGuire (2009).

3.2. Geochemical models of pyrite, calcite, and anorthite dissolution and modeling uncertainty

Results for the geochemical modeling of the potential pyrite dissolution during the Frio-I Brine Pilot experiment are shown in Fig. 3. The kinetic rate constant for the base case is 2.79×10^{-15} mol cm^{-2} s^{-1} calculated using Eq. (2) for the pH of 3.3 and dissolved oxygen of 3.5×10^{-6} molal. Taking into account the uncertainties in Eq. (2), for the given pH and dissolved oxygen values, the minimum and maximum rate constants are 1.24×10^{-15} and 6.26×10^{-15} mol cm^{-2} s^{-1}, respectively. Three models were constructed (a) base case model, $k = 2.79 \times 10^{-15}$ mol cm^{-2} s^{-1}, 89 g pyrite, and 3.5×10^{-6} mol kg^{-1} dissolved O_2; (b) $k = 3.02 \times 10^{-12}$ mol cm^{-2} s^{-1} (this k value is from Xu et al., 2010), 89 g pyrite, and 3.5×10^{-6} mol kg^{-1} dissolved O_2; and (c) $k = 2.79 \times 10^{-15}$ mol cm^{-2} s^{-1}, 171 g pyrite (maximum estimated based on the petrographic data), and 3.5×10^{-6} mol kg^{-1} dissolved O_2. Temperature was set at 25 °C in all cases. For the base case model (a) we also tested lower (1.24×10^{-15} mol cm^{-2} s^{-1}) and higher (3.26×10^{-15} mol cm^{-2} s^{-1}) rate constant values. The predicted Fe^{2+} concentrations from the three models fall roughly on the same line on the scale of the plot (Fig. 3A) and do not reproduce the observed increase in the concentration of iron in the monitoring well samples. The maximum predicted Fe^{2+} component concentration is 41 mg L^{-1}. The concentration of Fe^{2+} in the monitoring well was approximately the same (about 28 mg L^{-1}) for the first four samples collected during the injection of CO_2 (Table 1, "During CO_2

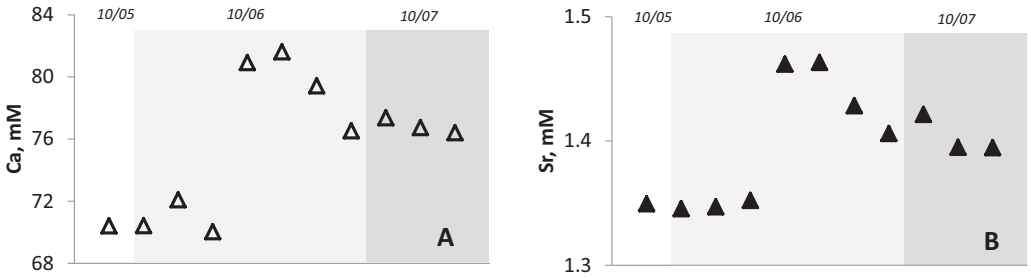

Fig. 2. Changes in the aqueous concentrations of (A) calcium, and (B) strontium in the monitoring well samples.

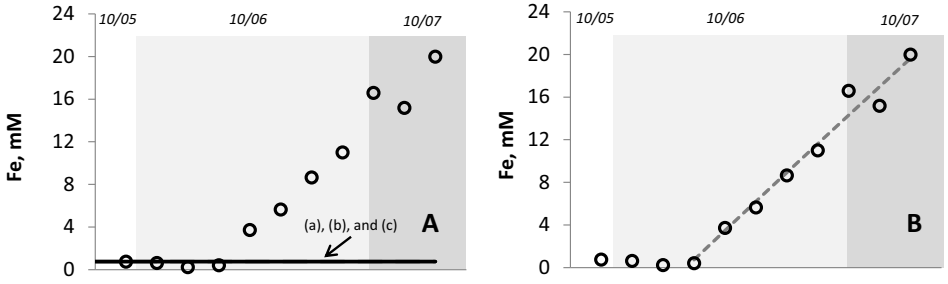

Fig. 3. Observed (points) and numerical models (lines) aqueous concentrations of Fe in the monitoring well. (A) Three reaction path models for pyrite considered here converged onto one line: (a) base case model, $k = 2.79 \times 10^{-15}$ mol cm^{-2} s^{-1}, 89 g pyrite, and 3.5×10^{-6} mol kg^{-1} dissolved O_2; (b) $k = 3.02 \times 10^{-12}$ mol cm^{-2} s^{-1}, 89 g pyrite, and 3.5×10^{-6} mol kg^{-1} dissolved O_2; and (c) $k = 2.79 \times 10^{-15}$ mol cm^{-2} s^{-1}, 171 g pyrite, and 3.5×10^{-6} mol kg^{-1} dissolved O_2. (B) Numerical model constructed to estimate the percentage of mass dissolved due to the dissolution of Fe(III) oxide (assumed hematite Fe_2O_3 stoichiometry). The model reasonably matches data if 1.5 g of hematite is allowed to dissolve during the Frio-I Brine Pilot test. This corresponds to 0.0169% of the considered rock mass. Temperature was set at 25 °C in all cases.

injection" section, and Fig. 3), and steadily increased to 1115 mg L^{-1} (Table 1).

Models (a) and (b) take into account the uncertainties in Eq. (2) and in the kinetic rate constants used in the other geochemical modeling studies; models (a) and (c) explicitly compare the uncertainly in the available mass of pyrite. All these uncertainties are insignificant, given the overall slow kinetics of pyrite dissolution (at the given low O_2 fugacity) compared to the duration of the experiment. Therefore, we conclude that dissolution of pyrite during the Frio-I Brine Pilot experiment is not a likely source of iron in the brine sampled from the observation well.

The amount of Fe^{2+} which can be released from pyrite is controlled by the availability of an oxidant (dissolved O_2). While dissolved O_2 was low (estimated at 3.5×10^{-6} mol kg^{-1}) during the Frio-I Brine Pilot, it may be higher in the future CO_2 injection scenarios. Oxygen content in the CO_2 captured from different sources varies widely—e.g., a typical range of 3–12 vol.% for the O_2 in the flue gas streams have been reported (Lee et al., 2009). Therefore, this potential geochemical response (dissolution of fine-grained pyrite) cannot be ignored in the injection scenarios where the CO_2 stream has appreciable amount of the O_2 impurity.

Xu et al. (2010) developed a calibrated model for Fe release during the Frio-I Brine Pilot test assuming desorption or dissolution of Fe(III) from the sediments. To estimate the percent of the mass loss from the sediment due to the release of iron, we constructed a geochemical model where we changed the mass of Fe(III) oxide hematite (as a proxy for Fe(III) oxyhydroxides) until the model reproduced the concentration of Fe observed in the monitoring well (Fig. 3B). A reasonable agreement between the observed values of dissolved Fe and model predictions was achieved when 1.5 g of Fe(III) oxide (hematite) was allowed to dissolve (Fig. 3B). This mass corresponds to 0.0169% of the considered rock mass.

Geochemical modeling results for calcite dissolution during the injection of CO_2 are shown in Fig. 4. The model agrees with the observations when the available mass of calcite is set at 0.5 g (0.0056 wt.% of the considered rock mass) and the dissolution rate constant at 10^{-8} mol cm^{-2} s^{-1}. Increasing temperature from 25 to 59 °C has a relatively minor impact on the Ca^{2+} concentration in brine (Fig. 4A) resulting in a difference in Ca^{2+} concentration of 1.6 molal. The results of evaluating calcite dissolution uncertainty are shown in Fig. 4B. The mass of calcite was varied between the likely values of 0.09 (0.001 wt.%) and 9.0 g (0.1 wt.%), and the calcite dissolution rate constants were varied from 10^{-8} to 10^{-10} mol cm^{-2} s^{-1}, as noted in Section 2. Due to low availability of calcite in the Frio Formation "C" sandstone, the change in the kinetic constant over two orders of magnitude has a relatively minor impact on Ca release. This very low (undetectable by XRD and petrographic examination) amount of calcite observed for Frio "C" sandstones would not be typical for other potential CO_2 sequestration sites in saline formations where calcite cement is usually abundant (Morad, 2009). Therefore, the uncertainty in the calcite dissolution rate constant will be significant for the rock assemblages with calcite on the order of a few wt.%. For example, our models constructed for 0.1 wt. % of calcite in sandstone (groups "a" and b" in Fig. 4B) and using two different rate constants ($k = 10^{-10}$ mol cm^{-2} s^{-1} and $k = 10^{-8}$ mol cm^{-2} s^{-1}) predict Ca^{2+} concentrations that are different by about 20 mM. While the concentration values are of the same order of magnitude, the physical result of this difference would be manifested in the total amount of rock mass dissolved after just 10 days

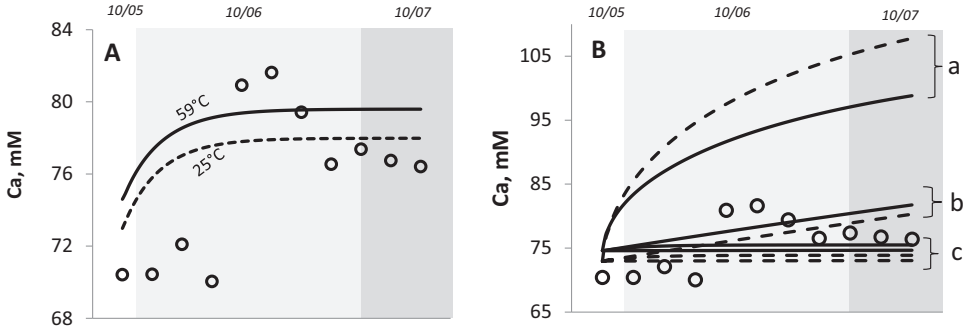

Fig. 4. (A) Changes in the aqueous concentration of Ca in the monitoring well (points) and proposed reaction path models (lines); the reaction path models assume Ca is released during kinetically controlled calcite dissolution, the mass of available calcite is set at 0.5 g, calcite dissolution rate constant $k = 10^{-8}$ mol cm^{-2} s^{-1}, dashed line—model calculated at 25 °C, solid line—at 59 °C; (B) difference between models' predictions assuming calcite dissolution rate constant values $k = 10^{-10}$ mol cm^{-2} s^{-1} and $k = 10^{-8}$ mol cm^{-2} s^{-1}, and mass of available calcite of 0.09 and 9.0 g. Dashed lines—models calculated at 25 °C, solid lines—at 59 °C. Group "a"—9 g $CaCO_3$, $k = 10^{-8}$ mol cm^{-2} s^{-1}, group "b"—9 g $CaCO_3$, $k = 10^{-10}$ mol cm^{-2} s^{-1}, group "c"—0.09 g $CaCO_3$, $k = 10^{-8}$ and 10^{-10} mol cm^{-2} s^{-1}.

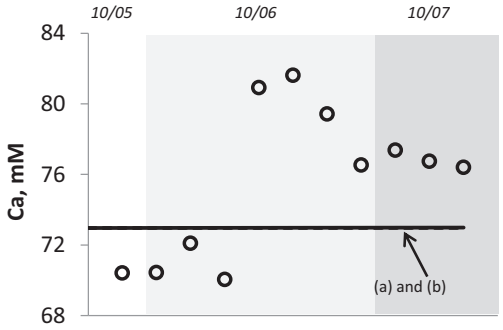

Fig. 5. Changes in the aqueous concentration of Ca in the monitoring well (points) and reaction path models (lines); these reaction path models assume Ca is released during kinetically controlled anorthite dissolution. The mass of available anorthite was set at 612 g, and the dissolution rate constants were (a) $k = 10^{-14.8}$ mol cm^{-2} s^{-1}, and (b) $k = 10^{-15.5}$ mol cm^{-2} s^{-1}. Temperature was set at 25 °C.

or reaction with CO_2: 0.027 wt.% for the faster rate constant ($k = 10^{-8}$ mol cm^{-2} s^{-1}) and only 0.007 wt.% for the slower rate constant ($k = 10^{-10}$ mol cm^{-2} s^{-1}).

Alternative reaction path models for interpreting the observed increase in Ca^{2+} concentration in the monitoring well are presented in Fig. 5. The geochemical models assume kinetically controlled dissolution of anorthite, which is present in the amounts detectable by XRD (McGuire, 2009). Due to the slow dissolution rates, the predicted increase in calcium concentration during the dissolution of anorthite cannot be reasonably matched to the monitoring well data at Frio-I. The dissolution rate constants used in two models were $10^{-14.8}$ and $10^{-15.5}$ mol cm^{-2} s^{-1}. The difference in calcium concentrations predicted using these two rate constants is insignificant (Fig. 5) due to the slow dissolution kinetics of this mineral relative to the duration of the test. Similar to the pyrite dissolution models, the temperature effect on the modeling outcome for anorthite dissolution was not examined because only specific ion interaction parameters at 25 °C are included in the Pitzer database (Jové Colón, 2005).

3.3. Reactive transport models

Results of the reactive transport modeling for the Frio-I experiment are illustrated in Fig. 6. The input values, the reacting fluid composition, minerals, and kinetic parameters for mineral dissolution are shown in Table 2.

The 1D radial reactive transport models predict the long-term mineral dissolution, including quartz, K-feldspar, oligoclase solid solution (1:4 anorthite:albite), calcite, and pyrite, and mineral precipitation, after the emplacement of CO_2 in the geochemical conditions representative of the Frio Formation "C" reservoir. The model captures the "relaxation" period, after CO_2 injection has been completed, and the system is allowed to achieve the original pH value of 6.7 after initially hosting the CO_2-saturated brine at pH 3.3. We compared four reactive transport models, constructed using two thermodynamic databases, and two temperatures (25 and 59 °C). The reactive transport models predict that carbonate minerals (dolomite and ankerite), as well as clay minerals (kaolinite, nontronite, and montmorillonite) precipitate in the Frio Formation "C" sandstone as the fluid-mineral system progresses toward equilibrium during a 1000-year period (Fig. 6). There is a difference in the mineral phases predicted to precipitate, depending on the thermodynamic database and activity correction model (thermo.dat with the B-dot activity model and Pitzer database compiled for this study). Both models are in agreement with regards to the predicted precipitation of kaolinite and dolomite, while Pitzer model also predicts montmorillonite and ankerite, and B-dot model- predicts nontronite precipitation. The four models are consistent in predicting the total volume of precipitating minerals.

The cumulative effect of uncertainties associated with using different thermodynamic databases, activity correction models, and extrapolating to the reservoir temperature are shown in Fig. 7. The

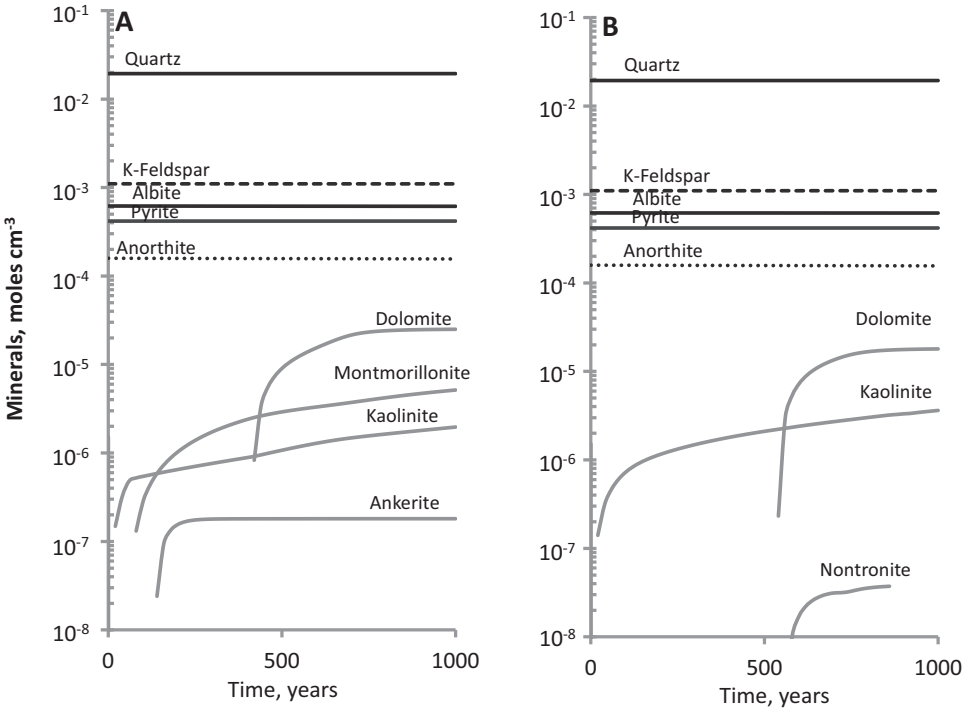

Fig. 6. Reactive flow models for 1000 years predict precipitation of clay minerals kaolinite, montmorillonite and nontronite, and carbonates dolomite and ankerite. Model "A" constructed using Pitzer activity correction model (database compiled for this study), and model "B" uses B-dot activity correction model (*thermo.dat*). Temperature was set at 59 °C for both models.

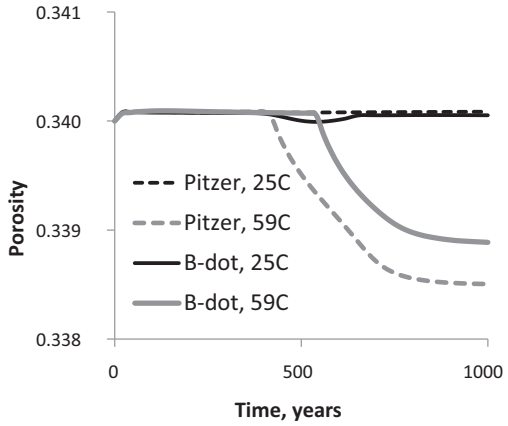

Fig. 7. Cumulative effect of uncertainties associated with using different thermodynamic databases, activity correction models, and extrapolating to the reservoir temperature. The uncertainties are evident in the total volume of predicted mineral precipitation, expressed as the change in the total porosity vs. time. The models using the B-dot activity correction are shown in black and gray solid lines, and Pitzer activity correction—in dashed lines.

uncertainties are expressed as the change in porosity which is a direct measure of the total volume of predicted mineral precipitation. The models constructed for 59 °C temperature predict a slight decrease in porosity due to mineral dissolution, and models constructed for 25 °C predict that porosity will not be affected. The difference in the final porosity predicted by the four models is within 0.002 vol.% (Fig. 7).

4. Conclusions—relevance to CO_2 sequestration in saline reservoirs

Based on the geochemical models and the selected geochemical data collected during the Frio-I Brine Pilot experiment, we conclude that: (1) increasing calcium and strontium concentrations in the monitoring well are best matched by the dissolution of trace amounts of calcite, whereas the dissolution kinetics of anorthite is too slow to account for the levels of observed calcium release; (2) pyrite dissolution is not a likely source of iron and manganese in the brine collected in the monitoring well; however, the long-term dissolution of pyrite provides Fe^{2+} for the precipitation of Fe-rich clay mineral nontronite; (3) dissolution of calcite and iron oxide resulted in ~0.02 wt.% loss of the considered rock mass during the Frio-I Brine Pilot test; (4) carbonate and clay mineral precipitation in the Frio Formation "C" sandstone is expected as the system progresses toward chemical equilibrium during a 1000 year period. Dolomite, ankerite, kaolinite, nontronite, and montmorillonite are expected to precipitate based on the reactive flow modeling calculations, with no significant effects on the overall reservoir porosity. Temperature (25 vs. 59 °C) had a relatively larger impact on the estimated mineral precipitation than using two different thermodynamic databases. The relatively low reactivity of the Frio "C" mineral assemblage causes geochemical reactions in this system to have minimal impact on total porosity, and therefore injectivity and long-term trapping.

This geochemical modeling study highlights potential sources of ions mobilized due to emplacement of $scCO_2$ in a subsurface reservoir, and includes an analysis of uncertainties in mineral dissolution rates and their impact on CO_2 sequestration in saline reservoirs. Uncertainties in the thermodynamic data and in the activity models for brines, and limitations in the applicability of dissolution (and precipitation) rates to complex natural systems, will most likely limit the accuracy of the geochemical models required to fully understand the geochemistry of carbon sequestration. Nonetheless, "calibrated" geochemical models, including reaction path and reactive transport simulations, can predict the complex mineralogy and brine chemistry resulting from the perturbation of a natural geological system by the injection of supercritical CO_2. Hence, geochemical models can provide insight on the impact of geochemical reactions on injectivity and long-term trapping, and can guide potential site selection based on the geochemistry of the site.

Acknowledgements

The authors acknowledge Susan Hovorka and Yousif Kharaka for the geochemical data from the Frio-I brine experiment, Carlos Jové-Colón for consultations with regards to the thermodynamic database, Katherine Klise for converting the Pitzer database into GWB format, and Mona Aragon for editing graphical abstract. This work was supported as part of the Center for Frontiers in Subsurface Energy Security, an Energy Frontier Research Center funded by the U.S. Department of Energy, Office of Science, Basic Energy Sciences under Award # DE-SC0001114. Sandia National Laboratories is a multi-program laboratory managed and operated by Sandia Corporation, a wholly owned subsidiary of Lockheed Martin Corporation, for the U.S. Department of Energy's National Nuclear Security Administration under contract DE-AC04-94AL85000.

References

Arvidson, R.S., Ertan, I.E., Amonette, J.E., Luttge, A., 2003. Variation in calcite dissolution rates: a fundamental problem? Geochim. Cosmochim. Acta 67, 1623–1634.

Bénézeth, P., Palmer, D.A., Anovitz, L.M., Horita, J., 2007. Dawsonite synthesis and reevaluation of its thermodynamic properties from solubility measurements: implications for mineral trapping of CO_2. Geochim. Cosmochim. Acta 71, 4438–4455.

Bénézeth, P., Dandurand, J., Harrichoury, J., 2009. Solubility product of siderite ($FeCO_3$) as a function of temperature (25–250 °C). Chem. Geol. 265, 3–12.

Bethke, C., 1998. The Geochemist's Workbench Release 3. 0. University of Illinois at Urbana-Champaign, Champaign, IL.

Bethke, C., 2008. Geochemical and Biogeochemical Reaction Modeling. Cambridge University Press, Cambridge, UK.

Bickle, M., Kampman, N., Wigley, M., 2013. Natural analogues. In: DePaolo, D.J., Cole, D.R., Navrotsky, A., Bourg, I.C. (Eds.), Geochemistry of Geologic CO_2 Sequestration.

DePaolo, D., Cole, D., Navrotsky, A., Bourg, I. (Eds.), 2013. Geochemistry of Geologic CO_2 Sequestration. MSA, GS.

Descostes, M., Vitorge, P., Beaucaire, C., 2004. Pyrite dissolution in acidic media. Geochim. Cosmochim. Acta 68, 4559–4569.

Doughty, C., Freifeld, B.M., Trautz, R.C., 2008. Site characterization for CO_2 geologic storage and vice versa: the Frio brine pilot, Texas, USA as a case study. Environ. Geol. 54, 1635–1656.

Drake, M.J., Weill, D.F., 1975. Partition of Sr, Ba, Ca, Y, Eu^{2+}, Eu^{3+}, and other REE between plagioclase feldspar and magmatic liquid: an experimental study. Geochim. Cosmochim. Acta 39, 689–712.

Druschel, G., Borda, M., 2006. Comment on "Pyrite dissolution in acidic media" by M. Descostes, P. Vitorge, and C. Beaucaire. Geochim. Cosmochim. Acta 70, 5246–5250.

Duan, Z., Sun, R., 2003. An improved model calculating CO_2 solubility in pure water and aqueous NaCl solutions from 273 to 533 K and from 0 to 2000 bar. Chem. Geol. 193, 257–271.

Fischer, C., Arvidson, R.S., Lüttge, A., 2012. How predictable are dissolution rates of crystalline material? Geochim. Cosmochim. Acta 98, 177–185.

Fitts, J.P., Peters, C.A., 2013. Caprock fracture dissolution and CO_2 leakage. In: DePaolo, D.J., Navrotsky, C.D.R., Bourg, A.I.C. (Eds.), Geochemistry of Geologic CO_2 Sequestration. , pp. 459–479.

Geng, M., Duan, Z., 2010. Prediction of oxygen solubility in pure water and brines up to high temperatures and pressures. Geochim. Cosmochim. Acta 74 (October (19)), 5631–5640.

Gilfillan, S.M.V., Sherwood Lollar, B., Holland, G., Blagburn, D., Stevens, S., Schoell, M., Cassidy, M., Ding, Z., Zhou, Z., Lacrampe-Couloume, G., Ballentine, C.J., 2009. Solubility trapping in formation water as dominant CO_2 sink in natural gas fields. Nat. Lett. 458, 614–618.

Haase, C., Dethlefsen, F., Ebert, M., Dahmke, A., 2013. Uncertainty in geochemical modeling of CO_2 and calcite dissolution in NaCl solutions due to different modeling codes and thermodynamic databases. Appl. Geochem., 306–317.

Harvey, O.R., Qafoku, N.P., Cantrell, K.J., Lee, G., Amonette, J.E., Brown, C.F., 2012. Geochemical implications of gas leakage associated with geologic CO_2 storage – a qualitative review. Environ. Sci. Technol. 47, 23–36.

Holland, T., Powell, R., 1998. An internally consistent thermodynamic data set for phases of petrological interest. J. Metamorph. Geol. 16, 309–343.
Jové Colón, C.F., 2005. Pitzer Database Expansion to Include Actinides and Transition Metal Species (data0.ypf.R1) (ANL-WIS-GS-000001 REV 00). U.S. Department of Energy, Office of Civilian Radioactive Waste Management, Office of Repository Development, Las Vegas, NV, USA, pp. 140.
Jun, Y.-S., Giammar, D.E., Werth, C.J., 2012. Impacts of geochemical reactions on geologic carbon sequestration. Environ. Sci. Technol. 47, 3–8.
Jung, H.B., Um, W., Cantrell, K.J., 2013. Effect of oxygen co-injected with carbon dioxide on Gothic shale caprock–CO_2–brine interaction during geologic carbon sequestration. Chem. Geol. 354, 1–14.
Kaszuba, J.P., Janecky, D.R., Snow, M.G., 2003. Carbon dioxide reaction process in a model brine aquifer at 200 °C and 200 bars: implications for geologic sequestration of carbon. Appl. Geochem., 1065–1080.
Kaszuba, J.P., Yardley, B., Andreani, M., 2013. Experimental perspectives on mineral dissolution and precipitation due to carbon dioxide–water–rock interactions. In: DePaolo, D.J., Navrotsky, C.D.R., Bourg, A.I.C. (Eds.), Geochemistry of Geologic CO_2 Sequestration. , pp. 153–188.
Kharaka, Y.K., Cole, D.R., 2011. Geochemistry of geologic sequestration of carbon dioxide. In: Harmon, R.S., Parker, A. (Eds.), Frontiers in Geochemistry: Contribution of Geochemistry to the Study of the Earth. Blackwell Publishing Ltd.
Kharaka, Y., Cole, D.R., Hovorka, S.D., Gunter, W., Knauss, K., Freifeld, B.M., 2006. Gas–water–rock interactions in Frio Formation following CO_2 injection: implications for the storage of greenhouse gases in sedimentary basins. Geology 34, 577–580.
Kharaka, Y., Thordsen, J.J., Hovorka, S.D., Nance, H.S., Cole, D.R., Phelps, T.J., Knauss, K.G., 2009. Potential environmental issues of CO_2 storage in deep saline aquifers: geochemical results from the Frio-I Brine Pilot test, Texas, USA. Appl. Geochem., 1106–1112.
Kharaka, Y., Cole, D.R., Thordsen, J.J., Gans, K.D., Thomas, R.B., 2013. Geochemical monitoring for potential environmental impacts of geologic sequestration of CO_2. In: DePaolo, D.J., Navrotsky, C.D.R., Bourg, A.I.C. (Eds.), Geochemistry of Geologic CO_2 Sequestration. MSA.
Kobos, P.H.A.C.M., Krumhansl, J.L., Dewers, T.A., McNemar, A., Borns, D.J., 2011. Combining power plant water needs and carbon dioxide storage using saline formations: implications for carbon diozide and water management policies. Int. J. Greenh. Gas Control, 899–910.
Land, L., 1984. Frio sandstone diagenesis, Texas Gulf Coast: a regional isotopic study. In: Clastic Diagenesis: AAPG Memoir 37., pp. 47–62.
Lee, J.-Y., Keener, T.C., Yang, Y.J., 2009. Potential flue gas impurities in carbon dioxide streams separated from coal-fired power plants. J. Air Waste Manag. Assoc. 59, 725–732.
Liu, F., Lu, P., Zhu, C., Xiao, Y., 2011. Coupled reactive flow and transport modeling of CO_2 sequestrationin the Mt. Simon sandstone formation, Midwest USA. Int. J. Greenh. Gas Control, 294–307.
Liu, F., Lu, P., Griffith, C., Hedges, S.W., Soong, Y., Hellevang, H., Zhu, C., 2012. CO_2–brine–caprock interaction: reactivity experiments on Eau Claire shale and a review of relevant literature. Int. J. Greenh. Gas Control 7, 153–167.
Lu, J., Kharaka, Y.K., Thordsen, J.J., Horite, J., Karamalidis, A., Griffith, C., Hakala, A.J., Ambats, G., Cole, D.R., Phelps, T.J., Manning, M.A., Cook, P.J., Hovorka, S.D., 2012. CO_2–rock–brine interaction in Lower Tuscaloosa Formation at Cranfield CO_2 sequestration site, Mississippi, USA. Chem. Geol., 269–277.
Marini, L., 2006. Geological Sequestration of Carbon Dioxide: Thermodynamics, Kinetics, and Reaction Path Modeling. Elsevier.
McGuire, K.A., 2009. CO_2 injection and reservoir characterization: an integrated petrographic and geochemical study of the Frio Formation, Texas. Ball State University.
Morad, S., 2009. Carbonate Cementation in Sandstones: Distribution Patterns and Geochemical Evolution (Special Publication 26 of the IAS). John Wiley & Sons.
Nitzsche, O., Mainrath, G., Merkel, B., 2000. Database uncertainty as a limiting factor in reactive transport prognosis. Contam. Hydrol., 223–237.
Pitzer, K.S., 1979. Theory: ion interaction approach. In: Pytkowicz, R.M. (Ed.), Activity Coefficients in Electrolyte Solutions. CRC Press, Boca Raton, FL, pp. 157–208.
Robie, R.A., Hemingway, B.S., 1995. Thermodynamic properties of minerals and related substances at 298.15 K and 1 bar (10^5 Pascals) pressure and at higher temperatures. US Geol. Surv. Bull. 2131, 461-461.
Sathaye, K.J., Hesse, M.A., Cassidy, M., Stockli, D.F., 2014. Constraints on the magnitude and rate of CO_2 dissolution at Bravo Dome natural gas field. Proceed. Natl. Acad. Sci. U. S. A. 111, 15332–15337.
Song, J., Zhang, D., 2012. Comprehensive review of caprock-sealing mechanisms for geologic carbon sequestration. Environ. Sci. Technol. 47, 9–22.
Steele-MacInnis, M., Capobianco, R.M., Dilmore, R., Goodman, A., Guthrie, G., Rimstidt, J.D., Bodnar, R.J., 2012. Volumetrics of CO_2 storage in deep saline formations. Environ. Sci. Technol., 79–86.
Stillings, L.L., Brantley, S.L., 1995. Feldspar dissolution at 25 °C and pH 3: reaction stoichiometry and the effect of cations. Geochim. Cosmochim. Acta 59, 1483–1496.
Williamson, M.A., Rimstidt, J.D., 1994. The kinetics and electrochemical rate-determining step of aqueous pyrite oxidation. Geochim. Cosmochim. Acta 58, 5443–5454.
Wolery, T.J., Jackson, K.J., Bourcier, W.L., Bruton, C.J., Viani, B.E., Knauss, K.G., Delany, J.M., 1990. Current status of the EQ3/6 software package for geochemical modeling. Chem. Model. Aqueous Syst. II 416, 104–116.
Xu, T., Apps, J.A., Pruess, K., 2004. Numerical simulation of CO_2 disposal by mineral trapping in deep aquifers. Appl. Geochem., 917–936.
Xu, T., Apps, J.A., Pruess, K., 2005. Mineral sequestration of carbon dioxide in a sandstone-shale system. Chem. Geol., 295–318.
Xu, T., Kharaka, Y.K., Doughty, C., Freifeld, B.M., Daley, T.M., 2010. Reactive transport modeling to study changes in water chemistry induced by CO_2 injection at the Frio-I Brine Pilot. Chem. Geol. 271, 153–164.
Xu, T., Zheng, L., Tian, H., 2011. Reactive transport modeling for CO_2 geological sequestration. J. Pet. Sci. Eng., 765–777.